IEEE Photonics Journal
An IEEE Photonics Society Publication

Open Access

Analysis of Mode Coupling Assisted Kerr Comb Generation in Normal Dispersion System

Volume 10, Number 5, September 2018

Shun Fujii
Yusuke Okabe
Ryo Suzuki
Takumi Kato
Atsuhiro Hori
Yoshihiro Honda
Takasumi Tanabe

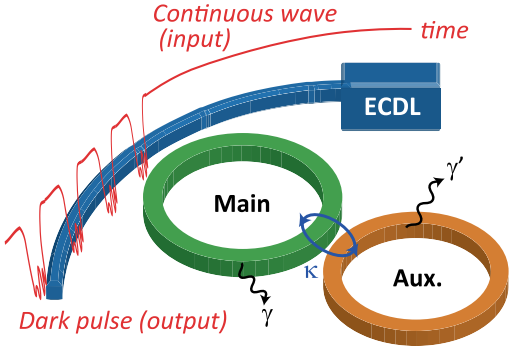

DOI: 10.1109/JPHOT.2018.2865417
1943-0655 © 2018 IEEE

IEEE photonics SOCIETY

IEEE

Analysis of Mode Coupling Assisted Kerr Comb Generation in Normal Dispersion System

Shun Fujii, Yusuke Okabe, Ryo Suzuki, Takumi Kato, Atsuhiro Hori, Yoshihiro Honda, and Takasumi Tanabe

Department of Electronics and Electrical Engineering, Faculty of Science and Technology, Keio University, Yokohama 223-8522, Japan

DOI:10.1109/JPHOT.2018.2865417

Manuscript received July 6, 2018; revised August 2, 2018; accepted August 10, 2018. Date of publication August 20, 2018; date of current version September 11, 2018. This work was supported in part by Ministry of Education, Culture, Sports, Science and Technology (MEXT), Photon Frontier Network Program and in part by JSPS (KAKENHI under Grant JP15H05429 and JP18J21797). Corresponding author: Takasumi Tanabe (e-mail: takasumi@elec.keio.ac.jp).

Abstract: By using nonlinear coupled mode equations, we numerically investigated the generation of a Kerr comb in a normal dispersion microcavity system, where mode coupling between two cavity modes is present. In contrast to previous studies, our model is rigorous in which we fully considered the mode coupling between two modes. We investigated the phase matching condition to obtain the suitable parameters needed to form a free-spectral-range (FSR)-selectable comb. Our calculations are in good agreement with existing experimental results, and enable us to obtain a good understanding of the phenomenon; moreover our model also allows us to reveal new phenomena. We investigated 1-FSR comb generation in detail and found that randomly oscillating behavior will appear when detuning is scanned, which has never before been clearly observed. This modeling approach will be a powerful tool that will assist dispersion engineering for Kerr comb generation and the frequency tuning needed to generate a deterministic mode-locked comb.

Index Terms: Kerr frequency comb, dark pulse, coupled cavities, nonlinear coupled mode equation.

1. Introduction

Kerr frequency comb generation is demonstrated using high-Q microcavities, which have been attracting considerable attention due to their various applications, which are thanks to its compactness, low power consumption, and high repetition rate [1]. One promising application is as light source for optical coherent telecommunications [2]–[4]. Kerr combs offer equally spaced spectrum lines of tens or even hundreds of gigahertz; and therefore, they have the potential for use in massively integrated optical communication systems. Recently, a data transmission experiment with a data stream exceeding 50 Tbit/s was demonstrated using a dissipative Kerr soliton comb in on-chip silicon nitride microresonators [3]. This work paves the way towards utilizing Kerr combs as chip-scale light sources in wavelength-division multiplexing. However, challenges still remain to be met before they can be used for practical applications. In particular, the conversion efficiency of the nonlinear process will limit its widespread use, because the reported conversion efficiency of a Kerr soliton comb in an anomalous dispersion regime is typically less than a few percent [5], [6],

and this results in the low power level of each comb line aggravating the noise figure and insertion loss.

In contrast to a mode-locked Kerr comb in an anomalous dispersion (i.e., a bright pulse), a mode-locked Kerr comb in a normal dispersion (i.e., a dark pulse) makes it possible to realize a much higher conversion efficiency than 30% in the infrared wavelength regime [7]. Although a normal dispersion has been considered unsuitable for Kerr comb generation due to a lack of modulation instability (MI) [8], [9], this issue has been solved by utilizing a mode coupling induced resonance frequency shift. It enables us to realize an anomalous local dispersion despite the overall dispersion being normal [10]–[13]. As a result, MI takes place in the coupled mode cavity system, and initial sidebands can be generated. Kerr comb generation via such a process will form a dark pulse, and it has been confirmed both experimentally and theoretically [11]–[13]. These previous studies have ensured that normal dispersion Kerr comb generation is attractive in terms of efficiency and the repeatability of soliton formation [11].

In this paper, we modeled and simulated the mode coupling assisted generation of a Kerr comb with a normal dispersion in a coupled cavity system by using nonlinear coupled mode equations (NCMEs). Although numerical simulations including the mode coupling effect have been conducted using Lugiato-Lefever equations [11], [13]–[16] and nonlinear coupled mode equations [17]–[20], there has been little work that has rigorously modeled the effect of mode-coupling-induced phase-matching on Kerr comb generation using two-mode equations. Even though a model with only single mode equation is rather simple and reduces calculation cost, the proposed model here (i.e., comb evolution including two different mode families) enabled us to simulate in a more rigorous way, and it allowed us to obtain optimized parameters in a practical experiment. In addition to reproducing the experimental results, we will discuss new findings related to the oscillating and non-oscillating behaviors of the optical spectrum during Kerr comb evolution, which are very sensitive to the chosen parameters.

This paper is organized as follows. In Section 2 we describe coupled mode equations (CMEs) that we used in our study. Section 3 shows a theoretical analysis where we discuss the phase matching condition of FSR-selectable Kerr comb generation using CMEs. Section 4 and 5 provide the simulation results of Kerr comb generation, which have been conducted based on the analysis of phase-matching condition described in Section 3. We provide a conclusion in Section 6.

2. Model

2.1 Coupled Cavity System

In this section, we describe the model that we used throughout this study. Figure 1(a) is a schematic illustration of the coupled cavity system of interest. The Main cavity is coupled with both an external waveguide and an Auxiliary (Aux.) cavity. The coupling rate between the Main and Aux. cavity modes given in angular frequency is κ. We denote the field amplitude of the Main and Aux. cavity modes with *a* and *b*. γ and γ' are the loaded decay rates (in angular frequency) of the two cavities, where the coupling rate with the external waveguide is also taken into account for γ.

The Aux. cavity is used to achieve mode coupling with the Main cavity. Figure 1(b) shows a diagram of the spectrum of the Main and Aux. cavities when two cavities are coupled at mode $\mu = -1$, where μ is an integer showing the relative longitudinal mode number. ω_μ and ω'_μ are the angular resonant frequencies of the longitudinal modes at mode number μ for the Main and Aux. cavities, respectively. The mode coupling induces two new supermode resonances with frequencies denoted by $\omega_\mu^{(-)}$ and $\omega_\mu^{(+)}$, where $\omega_\mu^{(-)}$ is the symmetric mode and $\omega_\mu^{(+)}$ is the anti-symmetric mode.

It should be noted that the free-spectral range (FSR) is not equidistance when the cavity system has dispersion, which means that the resonance asymmetry factor Δ_{as} is positive ($\Delta_{\mathrm{as}} > 0$) for an anomalous dispersion and negative ($\Delta_{\mathrm{as}} < 0$) for a normal dispersion, when it is defined as $\Delta_{\mathrm{as}} = (\omega_\mu - \omega_0) - (\omega_0 - \omega_{-\mu})$. The definition is the same way as in Ref. [12]. This is also the same definition that we used when we discussed the phase-matching condition of four-wave mixing with fourth-order dispersion [21].

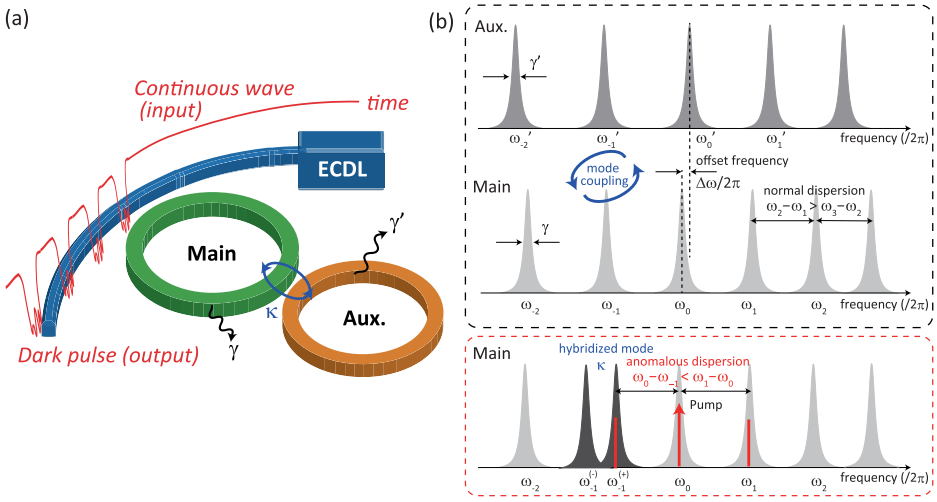

Fig. 1. (a) Schematic illustration describing the model of the coupled cavity system we used for this study. The Main cavity is pumped by a continuous wave laser, and the Aux. cavity is used to induce mode coupling. (b) Diagram showing the spectrum when two cavities are coupled at mode $\mu = -1$. The pump light is at $\mu = 0$.

The two cavities are both in a normal dispersion regime ($\Delta_{as} < 0$) but have slightly different FSRs and dispersions. To obtain mode coupling at the desired μ, the resonant angular frequency of the Aux. cavity mode at $\mu = 0$ (i.e., ω_0') is shifted slightly from that of the Main cavity (ω_0) with an angular frequency offset of $\Delta\omega$.

When the dispersion of the Main cavity is given, the resonance angular frequency at the relative mode number μ of a coupled Main cavity is given as $\omega_\mu = \omega_0 + \mu D_1 + (1/2)\mu^2 D_2$, where D_1 is the cavity-FSR, and D_2 is the second-order dispersion (dispersion is normal when $D_2 < 0$). Hence, the resonant frequencies of the Aux. cavity is shifted by $\Delta\omega$ from the Main cavity, for example $\omega'_\mu = (\omega_0 + \Delta\omega) + \mu D'_1 + (1/2)\mu^2 D'_2$ (the higher-order dispersions are neglected in our model). When the offset frequency $\Delta\omega$ is zero, the center frequency ω_0 is equal to that of the main mode, which means that the center modes ($\mu = 0$) of Main and Aux. are coupled. On the other hand, when the offset frequency has a nonzero value, the location at which the strong interaction occurs changes.

The system is pumped with continuous-wave (CW) laser light at mode $\mu = 0$. Although the overall dispersion is normal, the coupling between the Main and Aux. cavity modes will cause local anomalous dispersion ($\Delta_{as} > 0$) and make it possible to trigger the generation of the four-wave mixing (FWM). FWM light is generated followed by a cascade process and a Kerr comb is formed. Since the overall dispersion of the system is normal, the output exhibits a dark pulse [11].

As we describe in the following sections, we use coupled mode equations (CMTs) [22] to study the behavior of this model.

3. Theoretical Analysis

3.1 Supermode Resonance Induced by Mode Coupling

First, we start with a simple case, where a single mode is considered in Main and Aux. cavities, which are coupled together at a coupling rate of κ. The effect of the external waveguide is omitted. Then the CMT equations are given as [22], [23],

$$\frac{da}{dt} = \left(j\omega - \frac{\gamma}{2}\right) a + j\frac{\kappa}{2} b, \tag{1}$$

$$\frac{db}{dt} = \left(j\omega' - \frac{\gamma'}{2}\right) b + j\frac{\kappa}{2} a. \tag{2}$$

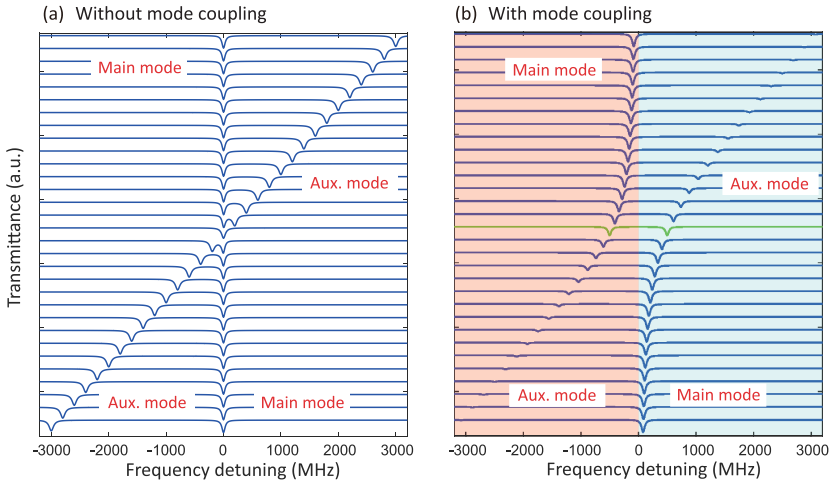

Fig. 2. Numerical investigation of transmittance (a) without and (b) with mode coupling ($\kappa/2\pi =$ 1000 MHz) when changing the frequency detuning of the auxiliary mode. Transmittance spectrum with same detuning of two resonances is shown by the green line in (b).

Note that the cavity decay rate, quality factor and resonance angular frequency are given as $\gamma = \omega/Q$.

In a steady state, the eigenvalues $\omega^{(\pm)}$ of the Eqs. (1), (2) are given as,

$$\omega^{(\pm)} = \frac{\omega + \omega'}{2} + \frac{j}{2}\left(\frac{\gamma}{2} + \frac{\gamma'}{2}\right) \pm \sqrt{\left[\frac{\omega - \omega'}{2} + \frac{j}{2}\left(\frac{\gamma}{2} - \frac{\gamma'}{2}\right)\right]^2 + \left|\frac{\kappa}{2}\right|^2}. \tag{3}$$

Figure 2 shows the theoretical transmission spectrum with and without a mode coupling effect when we change the detuning of the Aux. mode. (To be precise, the vertical axes are $|1 - \tilde{a} - \tilde{b}|^2$ and $|1 - \tilde{a}|^2$ for Figs. 2(a) and 2(b), respectively. $\tilde{a}$ and $\tilde{b}$ are the Fourier transformed spectra of the field amplitudes a and b, respectively.) The main mode is not affected when there is no mode coupling ($\kappa = 0$), and thus the resonant frequency does not exhibit anti-crossing behavior as shown in Fig. 2(a). When mode coupling ($\kappa/2\pi = 1000$ MHz) is present anti-crossing behavior is observed. The frequencies of the hybridized resonances are located at positions that are red- ($\omega^{(-)}$) and blue- ($\omega^{(+)}$) shifted in relation to the original resonance position as shown in Fig. 2(b) (see also Fig. 1(b)). When the detuning between two resonances is zero (green line), the mode splitting exhibits an angular frequency separation of κ ($=\omega_\mu^{(+)} - \omega_\mu^{(-)}$).

3.2 Phase-Matching Condition Induced by Mode Coupling

Next, we investigate the phase-matching condition needed to initialize the sideband generation. The relationship between three modes, namely the pump ω_0, signal $\omega_{-\mu}$ and idler ω_μ modes, are investigated in detail. As we described in Sec. 2, the resonance asymmetry factor Δ_{as} is used for the analysis.

Despite the overall dispersion of the system being normal, the local anomalous dispersion ($\Delta_{\text{as}} > 0$) due to the mode coupling makes MI gain possible at the desired mode number μ. As a result, FWM starts to occur. As we have already discussed, the frequency location of the local normal dispersion can be selectively changed by changing $\Delta\omega$ by tuning the resonance frequency of the Aux. mode. It is experimentally demonstrated that a deterministic generation of the arbitral FSR mode-locked Kerr comb is possible by changing the position of the mode coupling [12].

For instance, when $\Delta\omega$ is tuned in such a way that the mode coupling occurs at $\mu = 3$, the initial sidebands start to appear at a distance of 3-FSRs from the pump mode ($\mu = 0$); and with the help of the cascade process a mode-locked Kerr comb (dark pulse) with a 3-FSR spacing is formed. The above has been demonstrated by using dual-coupled silicon nitride microrings with integrated

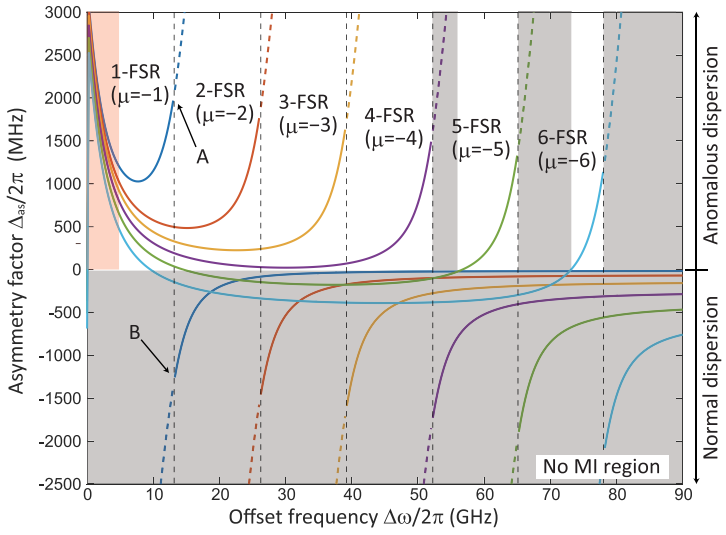

Fig. 3. Theoretical analysis of the asymmetry factor versus the offset frequency of the Aux. mode for each mode. The gray shaded region indicates no MI region because of the local dispersion being a normal dispersion. The asymmetry factor increases greatly for each mode number μ in the red shaded region ($\Delta\omega/(2\pi) = 0 \sim 5$ GHz).

heaters that allow to tune the resonance via the thermo-optic effect [12]. Such a system allows us to control the location of the initial comb lines, which in turn enables us to realize an FSR-selectable mode-locked Kerr comb in a normal dispersion.

Figure 3 shows the asymmetry factor Δ_{as} at different μ, as a fuction of $\Delta\omega$. κ is fixed at a constant value ($\kappa/2\pi = 3.34$ GHz). To obtain MI gain we need to satisfy the anomalous dispersion condition ($\Delta_{\text{as}} > 0$) whose area is shown in white in Fig. 3. The gray shaded region indicates the absence of MI gain due to the normal dispersion of the system.

As the offset frequency $\Delta\omega$ increases, the mode number μ where mode coupling occurs also increases. The vertical black dotted line represents $\Delta\omega$, when the Main and Aux. modes at μ perfectly overlap its resonant frequencies (i.e., $\omega_\mu = \omega'_\mu$) and couple. This means that the frequency separation between A and B in Fig. 3 is equal to $\kappa/(2\pi)$. When $\Delta\omega/(2\pi)$ approaches 12.5 GHz, the splitting ($\omega_{-1}^{(+)} - \omega_{-1}^{(-)}$) approaches maximum, and thus Δ_{as} is at its largest. This is because the anti-symmetric mode ($\omega_{-1}^{(+)}$) is shifted to its maximum from the original frequency ω_{-1}, and its mode is of interest because it will contribute to the positive Δ_{as}. When $\Delta\omega/(2\pi) =$ 12.5 GHz (at "A"), the energy of the hybridized mode is equally distributed between the Main and Aux. cavities. However, when $\Delta\omega/(2\pi)$ is larger than 12.5 GHz, the mode is stronger at the Aux. cavity and the anti-symmetric mode ($\omega_{-1}^{(+)}$) does not couple efficiently with the Main cavity (represented by the thin dotted curve in Fig. 3). Therefore, we now need to focus on the symmetric mode ($\omega_{-1}^{(-)}$), which contributes to the normal dispersion of the system (at "B").

When $\Delta\omega$ is small, we can always find a coupled mode exhibiting a local anomalous dispersion. However, when $\Delta\omega$ is large, we found that some ranges do not satisfy $\Delta_{\text{as}} > 0$. These features tell us that precise frequency tuning is needed if we require a local normal dispersion for high-FSR (i.e., 5-FSR, 6-FSR) comb generation.

On the other hand, the asymmetry factor for each mode number increases greatly when the offset frequency is close to zero (red shaded region), where the two center frequency modes ($\mu = 0$) are strongly coupled. In this region, we can no longer select the position of the initial comb sidebands because of the competition between the MI gains of different mode numbers μ. We will discuss this feature in Sec. 5.

Figure 4 shows further analysis of the phase-matching condition as a function of the mode coupling strength κ. This map shows that strong coupling (large mode splitting) makes it possible to

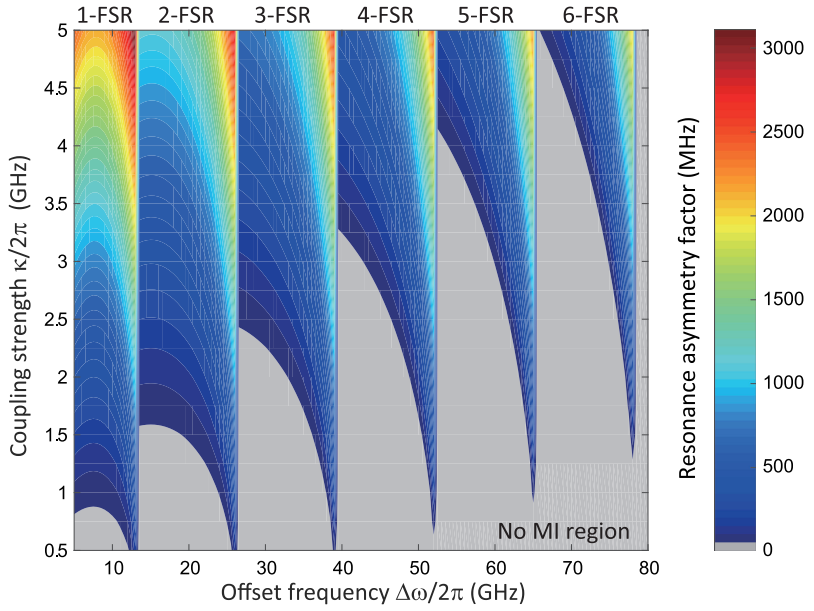

Fig. 4. Mapping of asymmetry factor versus offset frequency and coupling strength for different FSRs. The gray shaded region indicates th no MI region because of the local dispersion being normal dispersion. As the coupling strength increases, the no MI region becomes narrower because the phase-matching condition is easily satisfied.

have a large asymmetry factor and narrows the region with no MI gain. These analyses allow us to determine the critical condition as regards frequency tuning for FSR-selectable comb generation. The offset frequency gap from the 1-FSR to 6-FSR region is about 65 GHz when $\kappa/(2\pi) = 3.34$ GHz, which agrees with an experimental report on the frequency shift of the auxiliary mode ~64.8 GHz roughly estimated from the thermal heater power and the thermal shifting efficiency in Ref. [12].

4. Numerical Simulation

4.1 Nonlinear Coupled Mode Equations With Mode Coupling

Next we studied the behavior in detail by utilizing fully vectored coupled mode equations. The nonlinear coupled mode equations that we study are described as follows,

$$\frac{\partial a_\mu}{\partial t} = -\left[\frac{\gamma}{2} + i\left(\omega_\mu - \omega_p - \mu D_1\right)\right] a_\mu + ig \sum_{j,k} a_j a_k a^*_{j+k-\mu} + i\frac{\kappa}{2} b_\mu + f\delta_{\mu 0}, \tag{4}$$

$$\frac{\partial b_\mu}{\partial t} = -\left[\frac{\gamma'}{2} + i\left(\omega'_\mu - \omega_p - \mu D'_1\right)\right] b_\mu + ig' \sum_{j,k} b_j b_k b^*_{j+k-\mu} + i\frac{\kappa}{2} a_\mu, \tag{5}$$

where a_μ (Main) and b_μ (Aux.), respectively are the slowly varying amplitude of each comb mode. ω_p is the pump light frequency, and $g = \hbar\omega_0^2 n_2 D_1/(2\pi n_0 A_{\text{eff}})$ is the Kerr nonlinear coefficient at the Main cavity, where n_2, n_0, and A_{eff} are the nonlinear refractive index, refractive index, and effective mode area, respectively. The Kerr nonlinear coefficient g' at the Aux. cavity is defined in a similar way. $f = \sqrt{\gamma_{\text{ext}} P_{\text{in}}/(\hbar\omega_p)}$ is the external pumping term, and δ_0 is the Kronecker delta indicating that only $\mu = 0$ is pumped. The terms on the right-hand side in Eq. (4) represent the loss, cavity detuning and dispersion, the Kerr effect, mode couplings, and the external pump. In the following simulation, we calculated a total of 201 modes using the 4th-order Runge-Kutta method and a fast Fourier transform acceleration algorithm [24].

TABLE 1
Parameters Used for the Calculation in Section 4

Parameters	Symbol	Values (Main)	Values (Aux.)	Units
refractive index	n_0	1.98	1.98	-
nonlinear refractive index	n_2	2.4×10^{-19}	2.4×10^{-19}	m^2/W
center frequency	$\omega_0/(2\pi)$	191.9	191.9	THz
offset frequency	$\Delta\omega/(2\pi)$	-	*var. parameter*	GHz
cavity FSR	$D_1/(2\pi)$	378	391	GHz
dispersion	$D_2/(2\pi)$	-16	-17	MHz
effective mode area	A_{eff}	1.10	1.10	$\mu\mathrm{m}^2$
loaded quality factor	Q	7.5×10^5	3.7×10^5	-
external quality factor	Q_{ext}	3.5×10^6	-	-
mode coupling rate	$\kappa/(2\pi)$	3.34	3.34	GHz
input power	P_{in}	500	-	mW

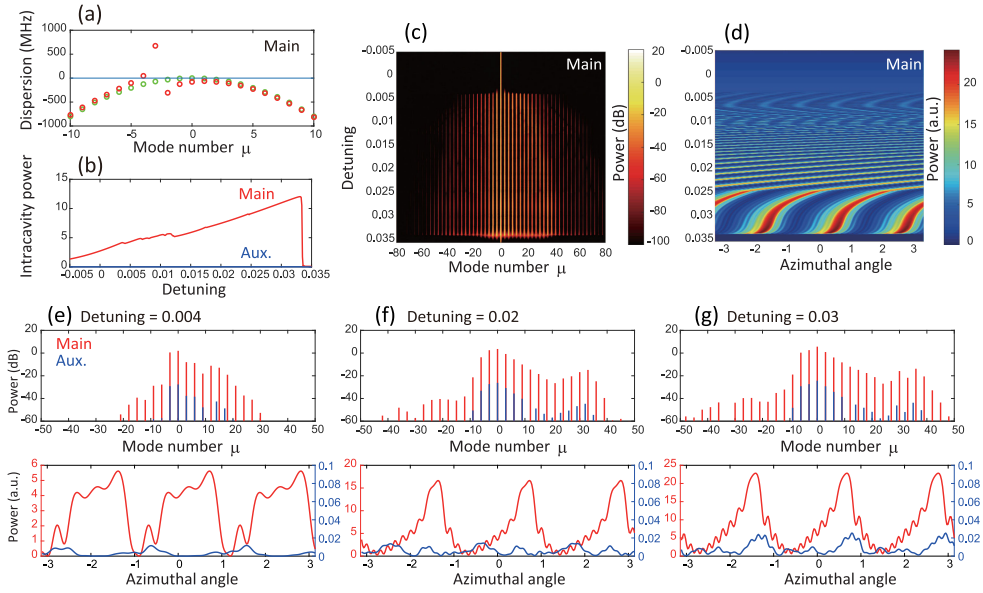

Fig. 5. (a) Cavity dispersion of the main mode with mode coupling (red circles) and without mode coupling (green circles). A strong mode interaction occurs in the mode number $\mu = -3$. (b) Average intracavity power and detuning during pump scanning from blue to red. The trajectory of the main mode follows the same path when the calculation is repeated with different initial noise conditions. (c,d) Evolution of the optical spectrum and time domain waveform versus detuning. (e–g) Simulated optical spectra and temporal waveforms of the main and auxiliary modes with different detunings.

4.2 FSR-Selectable Comb Simulation

To confirm the validity of our modeling, we first followed the experimental study by X. Xue *et al.* [12]. They used dual silicon nitride microrings with an integrated heater, which can facilitate the wavelength tuning of the auxiliary mode (i.e., tuning of $\Delta\omega$). The parameters are shown in Table 1, and are taken from Ref. [12].

Figure 5 shows the results of 3-FSR comb generation. The offset frequency is $\Delta\omega/(2\pi) = 36$ GHz, of which value is determined by the theoretical curve in Fig. 3. Figure 5(a) shows the cavity dispersion ($\omega_\mu - \omega_0 - \mu D_1$) of the coupled Main cavity, with (red) and without (green) mode couplings,

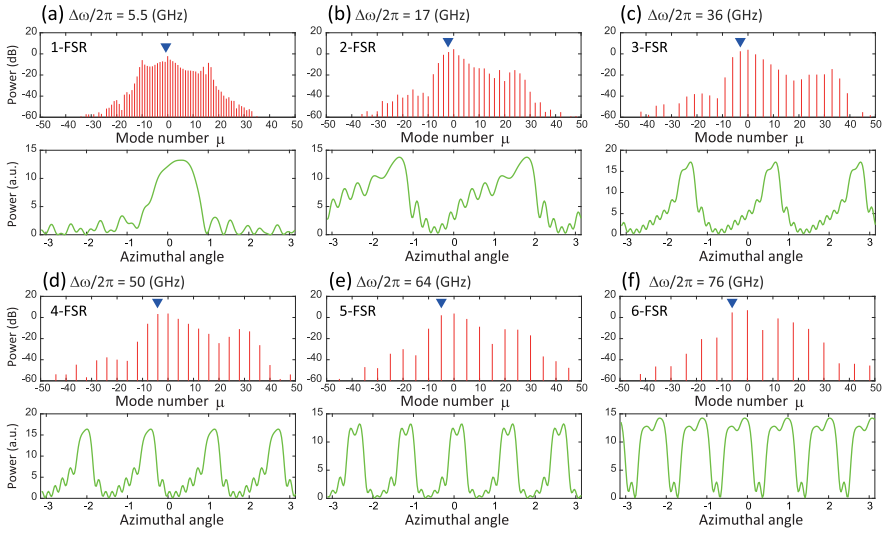

Fig. 6. Simulated optical spectra and temporal waveforms with different offset frequencies $\Delta\omega/(2\pi)$. The blue arrows indicate the locations of strong mode coupling. (a) 1-FSR; $\Delta\omega/(2\pi) = 5.5$ GHz. (b) 2-FSR; $\Delta\omega/(2\pi) = 17$ GHz. (c) 3-FSR; $\Delta\omega/(2\pi) = 36$ GHz. (d) 4-FSR; $\Delta\omega/(2\pi) = 50$ GHz. (e) 5-FSR; $\Delta\omega/(2\pi) = 64$ GHz. (f) 6-FSR; $\Delta\omega/(2\pi) = 76$ GHz.

indicating that a strong mode interaction is present in three mode apart from the pump mode. Figure 5(b–d),respectively show the average intracavity power, the evolution of the optical spectrum, and the temporal waveform at different normalized pump detunings $t_R(\omega_0 - \omega_p)$ (t_R is the roundtrip time of the Main cavity).

As reported in the previous work, the initial comb sidebands are generated at 3-FSR, where strong mode coupling occurred, and then a stable 3-FSR comb is formed without passing through a chaotic state. Even when we adopted different initial noise, the trajectory of the intracavity power followed the same path, which proved numerically that deterministic mode-locked dark pulse generation is indeed possible by using this scheme, as the authors in Ref. [12] claimed with respect to their experimental work.

Optical spectra and temporal waveforms at different pump detunings are shown in Fig. 5(e–g), where the red and blue lines represent the Main and Aux. modes, respectively. Azimuthal angle denotes the position along the circumference of the cavity, which is related to the fast time coordinates τ as $-D_1\tau$. When we increased the pump detuning, the dark pulse became broader (the spectrum bandwidth was also broader). As a result, the waveform had the appearance of a bright pulse-like state with periodic oscillatory tails. It is known as a platicon [18], although there are certain differences as we discuss later. They also show that the optical spectra exhibit an asymmetrical shape with respect to the pump mode. Usually, such trends are caused by the presence of higher-order dispersion (i.e., dispersive waves [25]), although we only included second-order dispersion in our model. The effect is present because we rigorously modeled the coupling that affects the effective dispersion profile of the Main cavity. The introduction of the mode coupling term enabled us to reproduce the reproduction of the asymmetric comb spectrum and the temporal waveform. This feature demonstrates the advantage of using a rigorous model instead of simply shifting the frequency of one of the modes of a single cavity [12].

Figure 6 shows the calculated results of multi-FSR comb generation. We obtained arbitrary-FSR comb generation simply by changing the offset frequency from 5.5 GHz to 76 GHz, which again agrees well with reported experimental results [12]. These results confirmed that our rigorous modeling is well suited for the simulation of Kerr comb generation in a coupled cavity system.

We note that some of the features we observed and describe in this paper were discussed in recent theoretical studies; oscillatory tails [13], and the change in angular pulse velocity depending on detuning [26]. In particular, the study reported by V. Lobanov *et al.* [18] is relevant to this work.

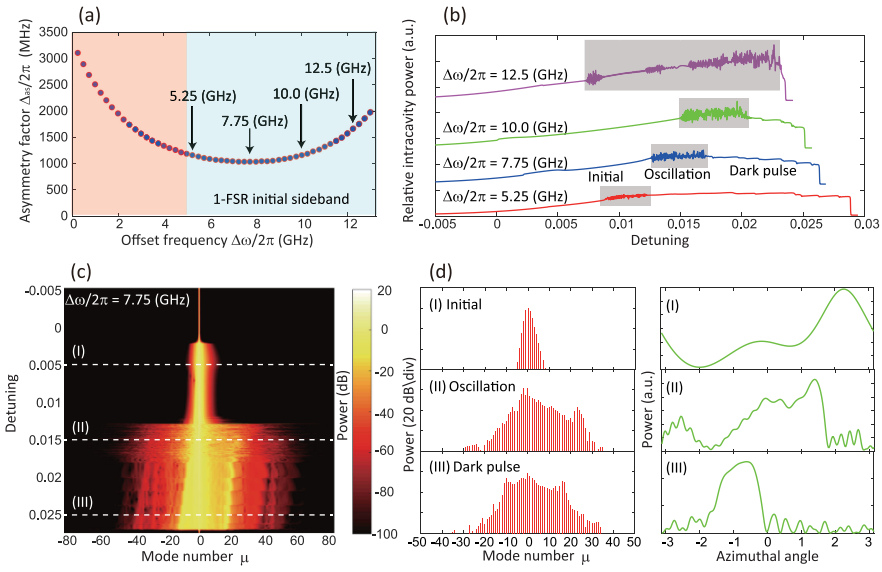

Fig. 7. (a) Asymmetry factor and offset frequency in the 1-FSR comb region. A 1-FSR sideband is generated as the initial comb in the blue shaded region, but a multi-FSR initial comb can be generated in the red shaded region. (b) Relative average intracavity powers with different offset frequencies. Oscillation behaviors were observed that depended on the chosen offset frequency. (c) Evolution of optical spectrum versus detuning with $\Delta\omega/(2\pi) = 7.75$ GHz. (d) Simulated optical spectra and temporal waveforms in each state in (c).

They undertook a numerical study of the generation of platicons. However, there are the following differences between their workand ours. They simulated coupling by introducing the shift of one of the modes [18], but we undertook rigorous modeling of the avoided crossing effect. So, they performed their calculation only for a Main cavity mode [18], whereas we fully calculated the two cavity modes, and so we took the energy transfer between the two cavity modes into account. Since recent studies have revealed that the energy transfer between coupled modes potentially affects soliton formation [27], we believe that our model will help us to study the formation of the comb spectra and time domain waveform in a realistic system in a more rigorous way.

5. Random Oscillating Behavior in 1-FSR Comb Generation

In this section, we investigate 1-FSR comb generation with different offset frequencies in more detail. Figure 7(a) is a magnified view of Fig. 3 for $\mu = 1$ (1-FSR), which shows the relation between the asymmetry factor Δ_{as} and the offset frequency $\Delta\omega$. First, we chose four different offsets ($\Delta\omega/(2\pi) = 5.25$, 7.75, 10.0, 12.5 GHz) and conduct a comb simulation. Figure 7(b) shows the calculated average intracavity power. It is noteworthy that randomly oscillating behaviors are observed whatever the offset frequency (gray shaded region). These behaviors have never before been observed for 3-FSR comb generation [see Fig. 5(b)], and the oscillating region is strongly dependent on detuning and offset frequency.

Figure 7(c) shows the evolution of the optical spectrum when we swept the pump detuning while setting $\Delta\omega/(2\pi)$ at 7.75 GHz. Snapshots of the spectrum and the waveform are shown in Fig. 7(d). In the initial state (I) (detuning $= 0.004 \sim 0.012$), the comb spectrum is stable but the bandwidth is relatively narrow. After the initial state, the optical spectrum becomes highly unstable. The intracavity power exhibits clear oscillations when the detuning is $0.012 \sim 0.017$ (II). Finally, it becomes stable again when detuning reaches 0.017. In this state, the intracavity power exhibits small steps, and the comb spectrum and temporal waveform show discrete transitions. These small steps have been observed experimentally in a normal dispersion system [11], although it is different from the soliton step usually observed in an anomalous dispersion system (corresponding to the change in soliton

number) [28]. In this condition, the comb repetition rate does not change from 1-FSR from start to end, and the temporal waveform in (III) is always in a mode-locked state even though the shape of the temporal waveform is similar to that of platicons.

When we locate the offset frequency in the blue shaded region in Fig. 7(a), initial sidebands are generated at 1-FSR. This is an expected behavior according to previous studies [10]–[12] since the 1-FSR resonant mode is the point at which a local dispersion change occurs. However, we observe a different trend (i.e., initial sidebands are generated at multi-FSRs) when we choose an offset frequency in the red shaded region. In this region, many resonant modes satisfy the phase matching condition simultaneously (see red shaded region in Fig. 3) because the pump mode exhibits a large red-shift due to the strong mode interaction between two center resonant modes. It has recently been reported that deterministic FSR generation in a normal dispersion system is not always possible even when using coupled cavities [29], and this may cause further discussion due to the contradictory observations reported in other studies [10]–[12]. Our analysis shows that both claims are correct and it is the matter of the parameters they employed, such as the coupling strength and frequency offset. In addition, our observation may suggest that such unstable (oscillating) behavior is related to such phenomena as the noisy comb state in 1-FSR comb generation.

6. Conclusion

In conclusion, we studied nonlinear coupled mode equations to simulate mode coupling assisted Kerr comb generation in a normal dispersion system. We investigated FSR-selectable comb generation by the employing a theoretical analysis and our calculation results agree well with experimental results reported in previous work. Moreover, we investigated the dynamics of oscillating behavior during detuning sweeping, which is very sensitive to the chosen parameter. The proposed model and analysis will be an aid to practical experiments on mode coupling assisted normal dispersion Kerr comb generation, in particular, the engineering and design of coupled cavities to obtain a desired Kerr frequency comb. The analysis of the phase-matching condition and calculation model proposed here can help us to understand practical experiments and allow us to control optical spectra and temporal waveforms.

Acknowledgment

We thank Dr. T. Miyaji for fruitful discussions.

References

[1] T. J. Kippenberg, R. Holzwarth, and S. A. Diddams, "Microresonator-based optical frequency combs," *Science*, vol. 332, no. 6029, pp. 555–559, Apr. 2011.
[2] J. Pfeifle *et al.*, "Coherent terabit communications with microresonator Kerr frequency combs," *Nature Photon.*, vol. 8, no. 5, pp. 375–380, May 2014.
[3] P. Marin-Palomo *et al.*, "Microresonator-based solitons for massively parallel coherent optical communications," *Nature*, vol. 546, no. 7657, pp. 274–279, Jun. 2017.
[4] A. Fülöp *et al.*, "Long-haul coherent communications using microresonator-based frequency combs," *Opt. Exp.*, vol. 25, no. 22, pp. 26678–26688, Oct. 2017.
[5] C. Bao *et al.*, "Nonlinear conversion efficiency in kerr frequency comb generation," *Opt. Lett.*, vol. 39, no. 21, pp. 6126–6129, Nov. 2014.
[6] P.-H. Wang *et al.*, "Intracavity characterization of microcomb generation in the single-soliton regime," *Opt. Exp.*, vol. 24, no. 10, pp. 10890–10897, May 2016.
[7] X. Xue, P.-H. Wang, Y. Xuan, M. Qi, and A. M. Weiner, "Microresonator Kerr frequency combs with high conversion efficiency," *Laser Photon. Rev.*, vol. 11, no. 1, pp. 1600276-1–1600276-7, Jan. 2017.
[8] M. Haelterman, S. Trillo, and S. Wabnitz, "Dissipative modulation instability in a nonlinear dispersive ring cavity," *Opt. Commun.*, vol. 91, no. 5, pp. 401–407, Aug. 1992.
[9] T. Hansson, D. Modotto, and S. Wabnitz, "Dynamics of the modulational instability in microresonator frequency combs," *Phys. Rev. A*, vol. 88, pp. 023819-1–023819-8, Aug. 2013.
[10] Y. Liu *et al.*, "Investigation of mode coupling in normal-dispersion silicon nitride microresonators for Kerr frequency comb generation," *Optica*, vol. 1, no. 3, pp. 137–144, Sep. 2014.
[11] X. Xue *et al.*, "Mode-locked dark pulse Kerr combs in normal-dispersion microresonators," *Nature Photon.*, vol. 9, no. 9, pp. 594–600, Aug. 2015.

[12] X. Xue *et al.*, "Normal-dispersion microcombs enabled by controllable mode interactions," *Laser Photon. Rev.*, vol. 9, no. 4, pp. L23–L28, 2015.
[13] J. K. Jang *et al.*, "Dynamics of mode-coupling-induced microresonator frequency combs in normal dispersion," *Opt. Exp.*, vol. 24, no. 25, pp. 28794–28803, Dec. 2016.
[14] X. Yi, Q.-F. Yang, X. Zhang, K. Y. Yang, X. Li, and K. J. Vahala, "Single-mode dispersive waves and soliton microcomb dynamics," *Nature Commun.*, vol. 8, pp. 14869-1–14869-9, Mar. 2017.
[15] G. D'Aguanno and C. R. Menyuk, "Coupled Lugiato-Lefever equation for nonlinear frequency comb generation at an avoided crossing of a microresonator," *Eur. Phys. J. D*, vol. 71, no. 3, pp. 74-1–74-7, Mar. 2017.
[16] S. Fujii *et al.*, "Effect on Kerr comb generation in a clockwise and counter-clockwise mode coupled microcavity," *Opt. Exp.*, vol. 25, no. 23, pp. 28969–28982, Nov. 2017.
[17] T. Herr *et al.*, "Mode spectrum and temporal soliton formation in optical microresonators," *Phys. Rev. Lett.*, vol. 113, Sep. 2014, Art. no. 123901.
[18] V. Lobanov, G. Lihachev, T. J. Kippenberg, and M. Gorodetsky, "Frequency combs and platicons in optical microresonators with normal GVD," *Opt. Exp.*, vol. 23, no. 6, pp. 7713–7721, Mar. 2015.
[19] A. B. Matsko, W. Liang, A. A. Savchenkov, D. Eliyahu, and L. Maleki, "Optical Cherenkov radiation in overmoded microresonators," *Opt. Lett.*, vol. 41, no. 13, pp. 2907–2910, Jul. 2016.
[20] X. Lei, Z. Gu, J. Ma, G. Qin, Z. Chen, and S. Chen, "Investigation of the local dispersion change in anomalous dispersion microcavity and quantitative analysis of the phase-matching in Kerr comb generation," *Appl. Opt.*, vol. 56, no. 16, pp. 4828–4834, Jun. 2017.
[21] S. Fujii, T. Kato, R. Suzuki, and T. Tanabe, "Third-harmonic blue light generation from Kerr clustered combs and dispersive waves," *Opt. Lett.*, vol. 42, no. 10, pp. 2010–2013, May 2017.
[22] H. A. Haus and W. Huang, "Coupled-mode theory," *Proc. IEEE*, vol. 79, no. 10, pp. 1505–1518, Oct. 1991.
[23] W. Yoshiki, A. Chen-Jinnai, T. Tetsumoto, and T. Tanabe, "Observation of energy oscillation between strongly-coupled counter-propagating ultra-high Q whispering gallery modes," *Opt. Exp.*, vol. 23, no. 24, pp. 30851–30860, Nov. 2015.
[24] T. Hansson, D. Modotto, and S. Wabnitz, "On the numerical simulation of Kerr frequency combs using coupled mode equations," *Opt. Commun.*, vol. 312, pp. 134–136, Sep. 2014.
[25] V. Brasch *et al.*, "Photonic chip-based optical frequency comb using soliton Cherenkov radiation," *Science*, vol. 351, no. 6271, pp. 357–360, Dec. 2016.
[26] V. E. Lobanov, A. V. Cherenkov, A. E. Shitikov, I. A. Bilenko, and M. L. Gorodetsky, "Dynamics of platicons due to third-order dispersion," *Eur. Phys. J. D*, vol. 71, no. 7, pp. 185-1–185-55, Jul. 2017.
[27] H. Guo *et al.*, "Intermode breather solitons in optical microresonators," *Phys. Rev. X*, vol. 7, pp. 041055-1–041055-10, Dec. 2017.
[28] T. Herr *et al.*, "Temporal solitons in optical microresonators," *Nature Photon.*, vol. 8, pp. 145–152, Dec. 2013.
[29] M. Karpov, M. H. P. Pfeiffer, J. Liu, A. Lukashchuk, and T. J. Kippenberg, "Photonic chip-based soliton frequency combs covering the biological imaging window," *Nature Commun.*, vol. 9, no. 1, pp. 1146-1–1146-8, Mar. 2018.